The Smallest Stable Fullerene, M@C$_{28}$ (M = Ti, Zr, U): Stabilization and Growth from Carbon Vapor

Paul W. Dunk,[†] Nathan K. Kaiser,[‡] Marc Mulet-Gas,[§] Antonio Rodríguez-Fortea,[§] Josep M. Poblet,*[,§] Hisanori Shinohara,[∥] Christopher L. Hendrickson,[†,‡] Alan G. Marshall,*[,†,‡] and Harold W. Kroto*[,†]

[†]Department of Chemistry and Biochemistry, 95 Chieftain Way, Florida State University, Tallahassee, Florida 32306, United States

[‡]Ion Cyclotron Resonance Program, National High Magnetic Field Laboratory, Florida State University, 1800 East Paul Dirac Drive, Tallahassee, Florida 32310, United States

[§]Departament de Química Física i Inorganica, Universitat Rovira i Virgili, c/Marcellí Domingo s/n, 43007 Tarragona, Spain

[∥]Department of Chemistry and Institute for Advanced Research, Nagoya University, Nagoya, 464-8602, Japan

S *Supporting Information*

ABSTRACT: The smallest fullerene to form in condensing carbon vapor has received considerable interest since the discovery of Buckminsterfullerene, C$_{60}$. Smaller fullerenes remain a largely unexplored class of all-carbon molecules that are predicted to exhibit fascinating properties due to the large degree of curvature and resulting highly pyramidalized carbon atoms in their structures. However, that curvature also renders the smallest fullerenes highly reactive, making them difficult to detect experimentally. Gas-phase attempts to investigate the smallest fullerene by stabilization through cage encapsulation of a metal have been hindered by the complexity of mass spectra that result from vaporization experiments which include non-fullerene clusters, empty cages, and metallofullerenes. We use high-resolution FT-ICR mass spectrometry to overcome that problem and investigate formation of the smallest fullerene by use of a pulsed laser vaporization cluster source. Here, we report that the C$_{28}$ fullerene stabilized by encapsulation with an appropriate metal forms directly from carbon vapor as the smallest fullerene under our conditions. Its stabilization is investigated, and we show that M@C$_{28}$ is formed by a bottom-up growth mechanism and is a precursor to larger metallofullerenes. In fact, it appears that the encapsulating metal species may catalyze or nucleate endohedral fullerene formation.
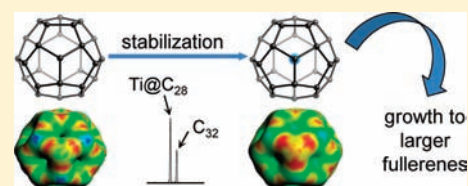
INTRODUCTION

Carbon is unique among the elements in the extraordinarily wide range and intricate complexity of its chemistry due to its facile bonding properties. Nowhere is this uniqueness more evident than in the variety of molecular structures that spontaneously form in carbon vapor. Morphological transitions as a function of increasing cluster size are observed from linear chains, to rings, and then finally to fullerenes, with less well characterized structures found as well.[1−4] Monocyclic ring structures dominate over linear chains at the C$_{10}$ cluster size;[2,3] however, the transition from rings to fullerenes is not well defined. Consequently, the smallest fullerene to form in carbon vapor is not known. That long-standing problem has received much interest since the discovery of C$_{60}$ because, for example, its identification can provide insight into fullerene formation and serve as a benchmark for experimental and theoretical studies. Furthermore, smaller fullerenes should possess fascinating properties that are distinct from those of their larger cousins. C$_{28}$, in particular, has been predicted to exhibit rich chemistry and form materials that possess exciting properties.[5−9]

Fullerenes are closed-cage carbon molecules consisting of 12 pentagons and any number of hexagons except one, and the smallest theoretically possible member is C$_{20}$. There is almost no evidence to suggest that this most strained fullerene,

comprised only of pentagons, forms spontaneously in carbon vapor; experimentally the monocyclic isomer dominates, although gas-phase detection of a very short-lived C$_{20}$ species has been claimed by debromination of C$_{20}$Br$_{20}$.[10] It is not topologically possible to construct a C$_{22}$ fullerene. Therefore, the smallest fullerene to form in carbon vapor is expected to be in the C$_{24}$−C$_{30}$ cluster region. Theoretical investigations predict that the stability from the ring to the fullerene structure may occur at C$_{26}$ or C$_{28}$,[11,12] but C$_{32}$ is the smallest fullerene observed to form in abundance (with very weak observations for C$_{30}$) under most experimental conditions.[3,4,13−15]

Early cluster beam experiments, however, provided circumstantial evidence that, under particular experimental conditions, fullerenes as small as C$_{24}$ may be stable enough to form and survive in carbon vapor, with a C$_{28}$ cluster being particularly abundant.[16] In the first theoretical study of small fullerenes,[5] the C$_{28}$ fullerene was suggested to explain the special abundance of that C$_{28}$ cluster. It was proposed to have a tetrahedral structure, Figure 1, unique among the smallest possible fullerenes (C$_{20}$−C$_{30}$) in that no more than three pentagons are directly fused. That structure minimizes the relative strain, potentially yielding enhanced stability over small

Figure 1. The structure originally proposed for a C_{28} fullerene. It contains four units of directly triple-fused pentagons arranged in tetrahedral symmetry.

fullerenes that must contain a more highly strained cage with four directly fused pentagons. The molecule was predicted to behave as a tetravalent "superatom" in which its four highly pyramidalized carbon atoms can be exohedrally stabilized by hydrogen to form $C_{28}H_4$. Further evidence in support of the C_{28} fullerene was provided by mass spectral investigations of soot prepared by the laser furnace and arc discharge methods.[17] That study suggested that C_{28} may be stabilized by uranium encapsulation. It also revealed that fragmentation of larger endohedral uranofullerenes appear to fragment by C_2 loss ("shrink-wrapping") below the C_{32} limit for empty cages for U@C_{28}. Still, it is not known if such a species can form directly in carbon vapor, and C_{28} has remained an important but elusive member of the fullerene family, relegated to the theoretical domain.[12,18−22] In fact, two subsequent experimental investigations of uranofullerenes did not find any evidence for U@C_{28}.[23,24]

Stabilization of C_{28} by an endohedral species is a fascinating prospect because it is known that fullerenes that cannot conform to the isolated pentagon rule[5] are stable enough to be macroscopically isolable by encapsulation with an appropriate

atom or moiety,[25−27] for example Sc_2@C_{66} and Sc_3N@C_{68}. Important factors for endohedral stabilization of medium to larger sized fullerenes are charge transfer from the encapsulating species to the fullerene cage and maximum separation of the pentagonal units in the molecular structure.[28,29] Thus, stabilization depends primarily on the electronic properties of the fullerene cage and the corresponding endohedral moiety, described as the ionic model,[28] as well as structural considerations. Our calculations on the T_d-C_{28} fullerene show agreement with previous investigations; it is an electronically open-shell system with the highest occupied molecular orbital (HOMO) essentially four-fold degenerate and occupied by four electrons. The T_d-C_{28} fullerene can avoid the most strained directly fused four-pentagon configuration, but its open-shell electronic structure with highly pyramidalized carbon atoms may render it too reactive to be observed under typical experimental conditions.

Electropositive metals that donate four electrons to the lowest unoccupied molecular orbital (LUMO) of the fullerene cage to afford a closed-shell M^{4+}@C_{28}^{4-} species with a large HOMO−LUMO gap, as a consequence of the energetically deep HOMOs, may permit sufficient stabilization for detection.[28] Gas-phase investigations probing such stabilization, however, have been hindered by the complexity of the mass spectra that result from non-fullerene clusters, empty cages, and endohedral fullerenes which all form spontaneously in carbon vapor.[30,31] That restriction is clearly illustrated in the case of titanium, an attractive tetravalent candidate for C_{28} stabilization by encapsulation. The major isotope, ^{48}Ti, differs in mass by only 52 mDa from C_4. Therefore, Ti@C_{28} would not be resolved from the empty-cage C_{32} with conventional mass spectrometers. In the present work, we use the pulsed laser cluster source technique directly coupled to a high-resolution Fourier transform ion cyclotron resonance (FT-ICR) mass spectrometer to investigate the formation and stabilization of
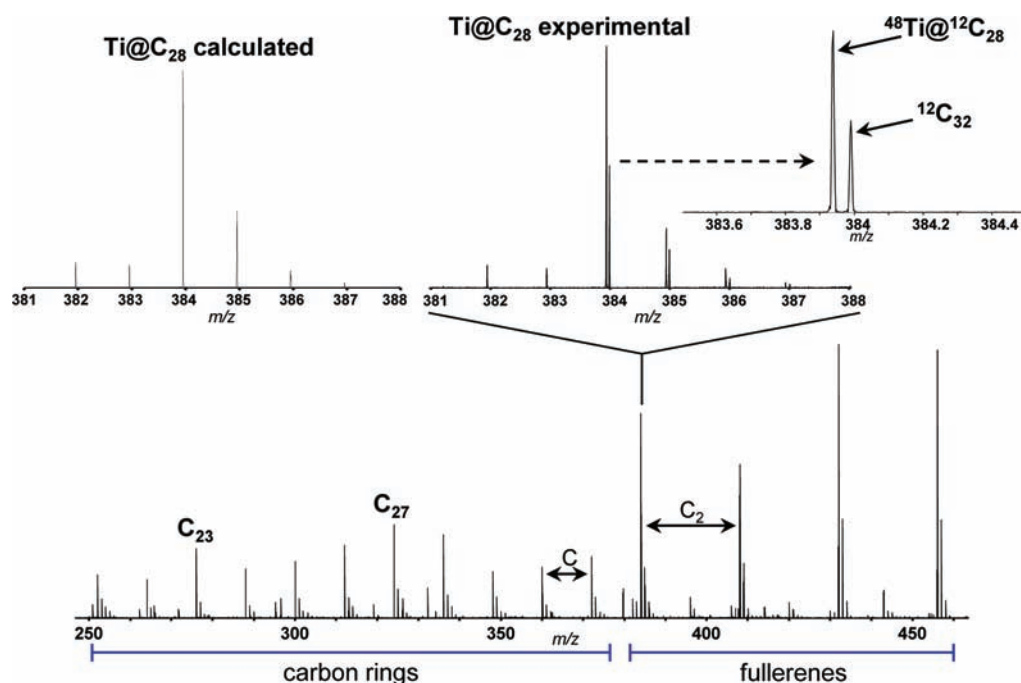

Figure 2. FT-ICR mass spectrum (positive ions) resulting from laser vaporization of a titanium-containing graphite target under conditions that probe the ring-to-fullerene transition. Ti@C_{28} forms as the smallest fullerene. The approximate 52 mDa mass difference between the smallest empty cage (C_{32}) and Ti@C_{28} is clearly resolved.

C_{28} and other small fullerenes.[32] We report the first experimental evidence for Ti@C_{28}, and stabilization of this smallest fullerene is also elucidated. An exhaustive investigation of elements across the periodic table was carried out for endohedral stabilization, and we found that only Zr and U additionally form M@C_{28} in abundance, with weaker formation for Hf@C_{28}. Our work further provides rare experimental insight into the formation of endohedral fullerenes and stabilization of small fullerenes. U@C_{28} is demonstrated to form in a bottom-up growth mode and is the precursor for larger uranofullerenes, which grow by the addition of atomic carbon and C_2 by the recently experimentally demonstrated closed network growth (CNG) mechanism.[33]

■ RESULTS AND DISCUSSION

Gas-Phase Synthesis and Detection of Ti@C_{28}. It is likely that any small, highly strained fullerenes will coalesce in the solid state or react upon exposure to solvent and air. Therefore, the molecular beam technique we use is most suitable for exploration of the smallest fullerenes because the species remain in the gas phase in a vacuum. Our experimental configuration is particularly powerful for such an investigation because the present 9.4 T FT-ICR mass spectrometer gives the highest resolution yet for the analysis of cluster source experiments.

In this work, many elements across the periodic table have been used to probe the formation of C_{28} (see Supporting Information). We find that only a few tetravalent metals sufficiently stabilize the C_{28} fullerene, and, in particular, Ti@C_{28} forms as a highly favored member of the M@C_{28} (M = group IV metal) fullerenes. Figure 2 shows the cluster cations formed from the laser vaporization of a titanium-doped (0.8% Ti) graphite target rod under conditions that probe the "ring-to-fullerene" structure transition region. Carbon rings appear to be dominantly observed in the C_{22}-to-C_{30} region as expected, evidenced by the higher abundance for C_{23} and C_{27} because the positive ion of monocyclic ring structures should exhibit enhanced stability (with $\Delta C_n = 4$) due to aromaticity. The pure carbon clusters in this mass region predominantly fragment by C_3 loss, for example C_{27} (see Figure S1, Supporting Information, and Figure 4, below), a characteristic of ring structures.[34,35] A cluster corresponding to Ti@C_{28} is revealed to be the most abundant molecular ion in the ring-to-fullerene transition region. Even-numbered fullerene species, Ti@C_{2n} and C_{2n}, dominate for larger clusters in the spectrum.

Figure 3 shows that the Ti@C_{28} cluster becomes even more abundant under cluster source conditions (higher He pressure) that most efficiently generate fullerenes. In fact, the Ti@C_{28} cluster has more than 3 times the relative abundance of the smallest empty cage, C_{32}. Under these conditions, the cyclic species are not observed, and fullerenes are exclusively detected. The distribution of Ti@C_{2n} shows that only Ti@C_{44} forms in higher abundance, further demonstrating that Ti@C_{28} exhibits special stability. Empty-cage fullerenes also form and exhibit a typical distribution in which C_{60} is the most abundant fullerene (not shown in the spectrum). However, Ti@C_{60} is weakly abundant, and most Ti metallofullerenes are small fullerenes. The empty cages exhibit greater relative abundances than the endohedral species, except for the smallest fullerenes. Titanium encapsulation appears to be an efficient method to produce the smallest fullerenes (C_{28}, C_{30}) that do not form in abundance as pristine cages. Calculated ionization
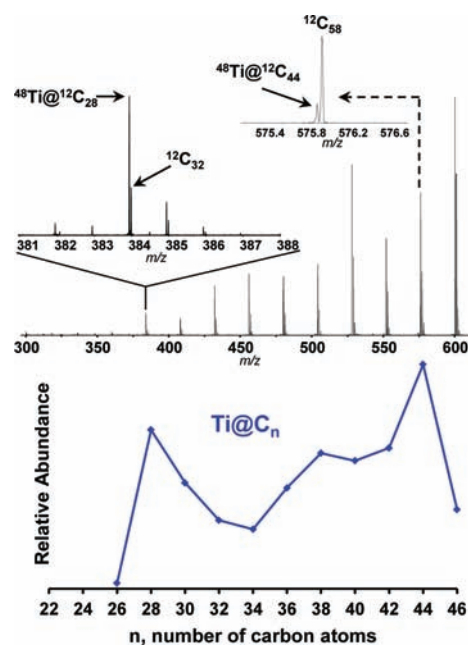

Figure 3. Cluster cations generated from vaporization of a Ti-doped graphite target under conditions that most efficiently generate fullerenes. Ti@C_{28} is observed to become more abundant and is particularly favored in the Ti@C_{2n} family. Note that empty-cage C_{28} is not observed.

potentials and electron affinities for the smallest species are given in the Supporting Information.

Collision-induced dissociation (CID) experiments were performed to confirm that the metal is located within the fullerene cage. The fragmentation pattern of a fullerene is unique among the various structural forms of carbon clusters because, when excited to high internal energy, loss of neutral C_2 units occurs with retention of the encapsulated metal. In contrast, carbon rings and linear chains predominantly fragment by loss of the more stable neutral C_3 molecule and loss of the metal atom if present. The very different fragmentation pathways allow structural identification in the gas phase.

Ti@C_{28} is isolated by the application of a stored-waveform inverse Fourier transform (SWIFT)[32] event that ejects all species except for Ti@C_{28} (and C_{32}) from the ICR cell (Figure S2, Supporting Information). The isolated molecular ions are subsequently excited to higher kinetic energy by applying an off-resonant radiofrequency. The ions then undergo many collisions with helium or argon to achieve high internal energies above the threshold energy for dissociation, and all resulting product ions are detected (see Experimental Section). Ti@C_{28} remains completely intact without loss of Ti after many collisions with He or Ar at kinetic energies of several kiloelectronvolts, and the cluster does not fragment by C_3 or C. Thus, the metal is not bound to the outside of the cage, and the molecular structure is neither linear nor cyclic. The molecule is determined to be remarkably stable after even greater thermal excitation via many collisions at higher kinetic energies (>10 keV), in accordance with an endohedral fullerene structure (Figure S2, Supporting Information). It is also clear that Ti@C_{28} is unable to fragment to a smaller fullerene.

Ti@C_{30} is also probed by CID, as shown in Figure 4, and fragmentation of C_{27} is also shown for comparison. C_{27} clearly fragments predominantly by C_3 loss, demonstrating that it is a
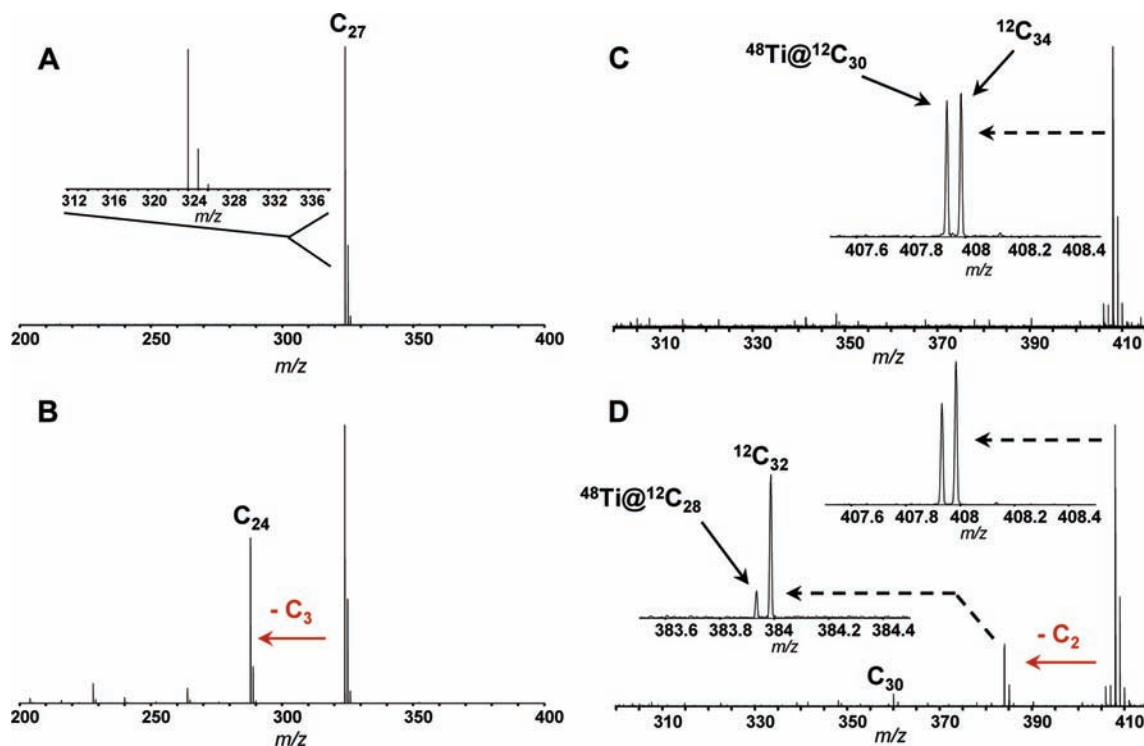
Figure 4. Comparison of fragmentation distributions for the C_{27} and Ti@C_{30} cluster cations. SWIFT-isolated C_{27} (A) and fragmentation pattern of C_{27} clearly shows C_3 loss, indicating it is a ring structure (B). SWIFT-isolated Ti@C_{30} and C_{34} (C) and fragmentation pattern of Ti@C_{30} (D). Ti@C_{30} fragments by C_2 loss with retention of the encapsulated Ti atom, clearly demonstrating that both Ti@C_{30} and Ti@C_{28} are endohedral metallofullerenes. Empty-cage C_{34} fragments by C_2 loss to C_{32} and C_{30}.

ring structure rather than a fullerene. It is not possible to isolate Ti@C_{30} from the empty C_{34} due to their very small mass difference. Therefore, Ti@C_{30} and C_{34} are isolated together to probe fragmentation behavior of Ti@C_{30}, as shown in Figure 4c. It is observed that Ti@C_{30}, when highly excited, primarily fragments by C_2 loss with retention of the encapsulated metal to Ti@C_{28}. That observation is considered as highly compelling evidence that it is an endohedral metallofullerene. The result further confirms that Ti@C_{28} and the other Ti@C_{2n} species are fullerenes with encapsulated metals. Further, the empty-cage C_{34} cluster fragments by C_2 loss to C_{32} and C_{30} (see also Figure S3, Supporting Information). Fragmentation of larger Ti@C_{2n}, for example Ti@C_{38} (Figure S4, Supporting Information), exhibits the same C_2 loss pattern. The abundance of Ti@C_{28} formed by fragmentation of larger endohedral metallofullerenes is low, suggesting that it is not formed as result of a fragmentation during the growth process.

In our experiments, M@C_{28} is detected only by encapsulation with group IV metals and U. Zr@C_{28} is observed to form in abundance but is less favored in the Zr@C_{2n} family than Ti@C_{28}, as shown in Figure 5. Hf@C_{28} appears to form much more weakly (Figures S5 and S6, Supporting Information) and also requires high resolution to detect because there are several molecular ions of its same nominal mass. A non-fullerene, inorganic Hf$_2$-based cluster forms in much more abundance than the weakly detected Hf@C_{28}.

Structure and Stabilization of Ti@C_{28}. Having established that Ti@C_{28} is an endohedral fullerene, we turn our attention to its cage structure and how the encapsulated metal may stabilize such a small and highly strained fullerene. One disadvantage for gas-phase investigations is that the common techniques that provide detailed structural information, such as
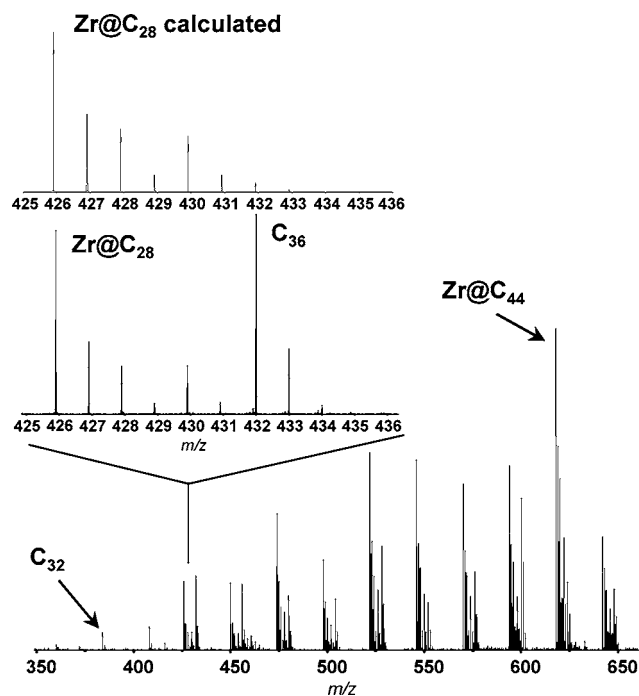

Figure 5. Small endohedral fullerenes formed by vaporization of a Zr-containing (0.8%) carbon rod. Zr@C_{28} is the smallest endohedral fullerene formed, whereas C_{32} is the smallest empty cage. Zr@C_{28} is not as favored as Ti@C_{28}.

NMR and X-ray diffraction, are not applicable. However, a closed-cage solution to C_{28} requires that the fullerene must possess 12 pentagons and four hexagons. Consequently, there
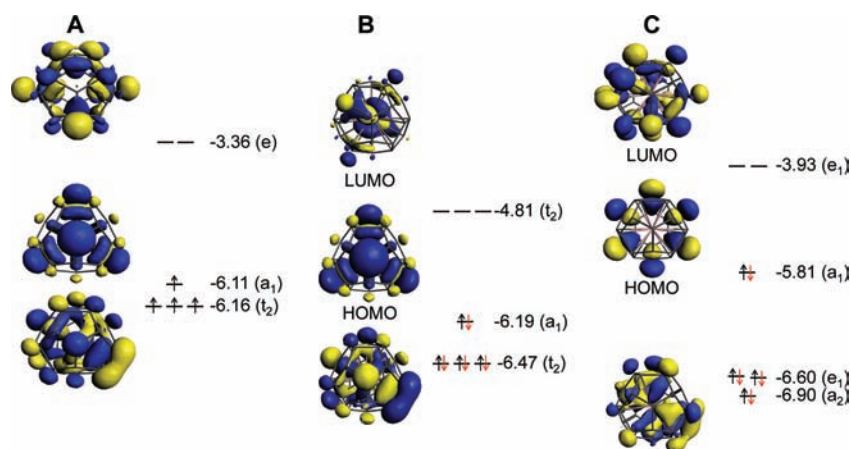
Figure 6. Frontier orbitals computed from DFT calculations for the tetrahedral isomer of C_{28} (A), and the corresponding endohedral Ti@T_d-C_{28} cluster with Ti centered within the cage (B) and Ti occupying an off-center position within the cage (C). Electrons transferred from the Ti atom to the carbon cage are highlighted in red.

are only two possible isomers (T_d or D_2 symmetry) for the C_{28} fullerene.[36] We have carried out theoretical investigations to discern the molecular structure and elucidate the factors that govern the stabilization of Ti@C_{28} and other small fullerenes.

Ti@C_{28} exhibits high relative abundance, but empty-cage C_{28} is not observed in our experiments, indicating that encapsulation of titanium significantly stabilizes the C_{28} fullerene cage. The T_d-C_{28} isomer possesses four units of directly fused triple pentagons in the structure, whereas D_2-C_{28} contains a much more highly strained pentagon configuration with four directly abutting pentagons. The ground state of the neutral T_d isomer is quintuplet, whereas the D_2 is singlet. That observation suggests that only for the T_d-C_{28} structure can an endohedrally located atom donate four electrons to the cage to form a species that is electronically closed shell with a large HOMO−LUMO gap, due to the low energy of the singly occupied orbitals. The electronic structure and frontier orbitals involved are shown in Figure 6 for T_d-C_{28} and in Figure S7 for the D_2 species. We find that the presence of the four energetically deep quasi-degenerate singly occupied molecular orbitals for the T_d isomer, which receive the four electrons from Ti, results in much stronger stabilization than for the D_2 isomer. Accordingly, the HOMOs for Ti@T_d-C_{28} show much lower energies than those for Ti@D_2-C_{28}. Therefore, in good agreement with a monoelectronic picture, Ti encapsulation renders the T_d isomer much more stable than the D_2 isomer. Indeed, the energy difference between the neutral empty-cage species is about 17 kcal·mol^{-1}, but this difference increases for the tetra-anion and Ti@C_{28} endohedral species to 61 and 55 kcal·mol^{-1}, as shown in Table 1.

Previous studies found that transferred charge to a fullerene cage is preferentially located at the most strained bonds, corresponding to the most pyramidalized atoms.[29] In T_d-C_{28}, those carbon atoms are located at the directly fused triple-pentagon junctions. Transferred charge is found to reside at the [5,5] bonds of these triple-fused pentagons, as shown in Figure 7. The T_d-C_{28} isomer has an optimal structure to accommodate the four electrons that minimizes Coulomb repulsion.

The Ti trapped inside the cage prefers nucleophilic regions of the fullerene. We find a significant interaction with the cage resulting in additional stabilization, as shown in Figure 8. A large energy difference between the endohedral metallofullerene with the Ti atom in the center of the cage and that with a

Table 1. Relative Energies for C_{28}, C_{30}, and C_{32} Empty Cages and Endohedral Ti@C_{2n} Clusters[a]

cage	isomer	C_{2n}	C_{2n}^{4-}	Ti@C_{2n}	N_p[b]
C_{28}	$D_2(1)$	17.5	61.6	54.9[c]	20
	$T_d(2)$	0.0	0.0	0.0[c]	18
C_{30}	$D_{5h}(1)$	49.7	58.6	62.9	20
	$C_{2v}(2)$	2.6	17.6	20.1	18
	$C_{2v}(3)$	0.0	0.0	0.0	17
C_{32}	$C_2(1)$	51.6	16.3	15.5	16
	$D_2(2)$	62.5	39.4	35.1	18
	$D_{3d}(3)$	66.1	29.1	31.0	18
	$C_2(4)$	24.5	1.8	4.0	17
	$D_{3h}(5)$	77.8	58.6	69.0	18
	$D_3(6)$	0.0	0.0	0.0	15

[a]Energies in kcal·mol^{-1}. [b]N_p is the total number of pentagon adjacencies. [c]The energy differences for encapsulated Zr or Hf are 75.0 and 73.2 kcal·mol^{-1}.

shift from the center is found. Ti@T_d-C_{28} with its Ti atom shifted is about 37 kcal·mol^{-1} lower in energy than when the Ti resides in the center. The displacement of the Ti atom toward the nucleophilic region from the center of the molecule is approximately 0.535 Å. The frontier orbitals (see Figure 6) also are significantly affected by the shift of the encapsulated metal. Similar results are found for M = Zr and Hf, with M@T_d-C_{28} much more favored than M@D_2-C_{28} (see Table 1). Interestingly, the Zr atom is also slightly displaced from the center of the cage toward the triple-fused pentagons (0.223 Å), but the Hf atom remains almost in the center of the fullerene.

Ionic Model for Small Fullerenes. To determine if the ionic model is also valid for other members of the Ti@C_{2n} family, DFT calculations were conducted for all isomers[36] of C_{30} and C_{32}. Relative energies are given in Table 1. As observed for C_{28}, neutral fullerenes and tetra-anions have rather different energies, although the most stable fullerene for both states corresponds to the cage isomer with a lower number of fused pentagons (N_p). In general, the energy difference between the cage isomers with different N_p is reduced when those cages are negatively charged. The greater extent of localization of negative charge on the most pyramidalized carbon atoms of the fused pentagons provides enhanced stabilization.[29,37] It is interesting to note that this behavior is also observed for the C_{30} and C_{32} families (Table 1), although it is more pronounced
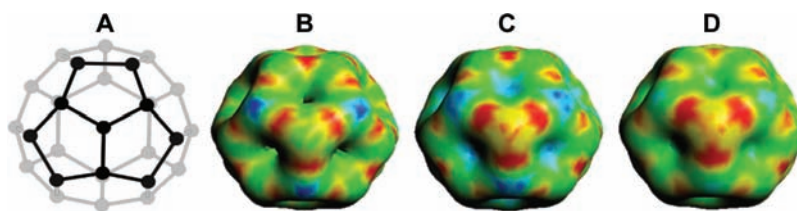
Figure 7. Representation of the structure of the T_d-C_{28} cage (A) and the molecular electrostatic potentials for the neutral T_d-C_{28} (B), tetra-anionic T_d-C_{28}^{4-} (C), and endohedral Ti@T_d-C_{28} (D) systems (with the Ti atom placed in the center of the cage). The charge transferred from the encapsulated Ti is localized at the four most pyramidalized carbon atoms in the T_d-C_{28} fullerene. The molecular structure is optimal to accommodate four electrons.
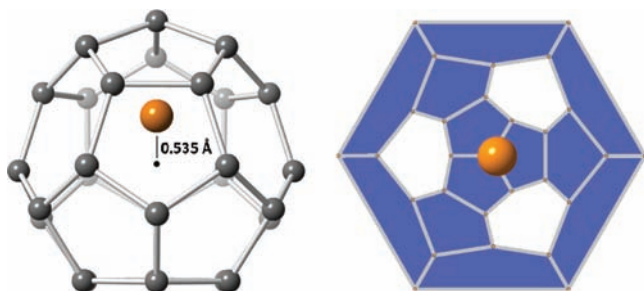

Figure 8. Molecular and Schlegel representations of Ti@T_d-C_{28}. The internally located Ti atom is located off-center, yielding additional stabilization.

for C_{28} due to the characteristic electronic structure of the T_d-C_{28} cage.

Comparison of the energies of C_{2n}^{4-} and Ti@C_{2n} clearly shows the validity of the ionic model for these larger systems. For C_{30}, we predict $C_{2v}(3)$-C_{30} (Figure 9) to be the preferred cage that encapsulates the Ti atom among the three possible isomers (Table 1). For the C_{32} family, the two most stable candidates are found within 4 kcal·mol^{-1} of each other: namely, cages $C_2(1)$-C_{32} and $D_3(6)$-C_{32}. Computation of the relative free energies and molar fraction distributions at different
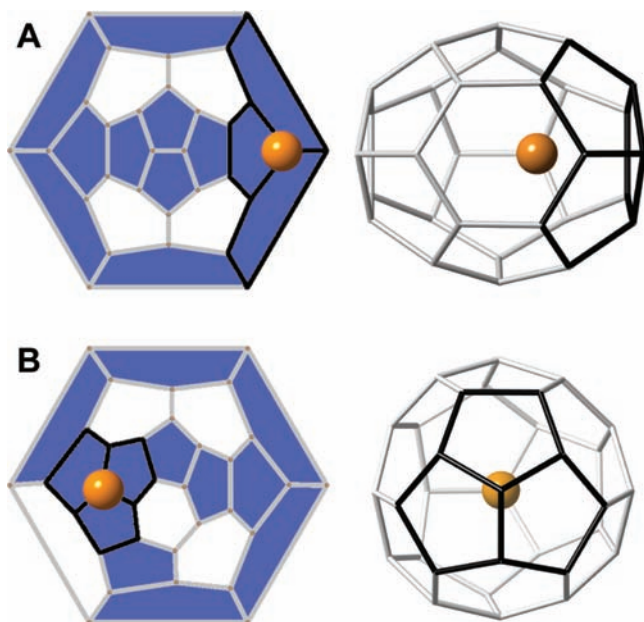

Figure 9. Schlegel and ball-and-stick representations of Ti@$C_{2v}(3)$-C_{30} (A) and Ti@$D_3(6)$-C_{32} (B), the predicted preferred isomers for Ti encapsulation of C_{30} and C_{32}.

temperatures, within the rigid rotor and harmonic approximation,[38,39] predicts Ti@$D_3(6)$-C_{32} (Figure 9) to be the most abundant isomer for the entire range of temperatures (Figure S8, Supporting Information).

U@C_{28}: Bottom-Up Formation of M@C_{28}. In addition to group IV metals, we find that uranium also forms M@C_{28}. Figure 10 shows the distribution of fullerenes produced by laser
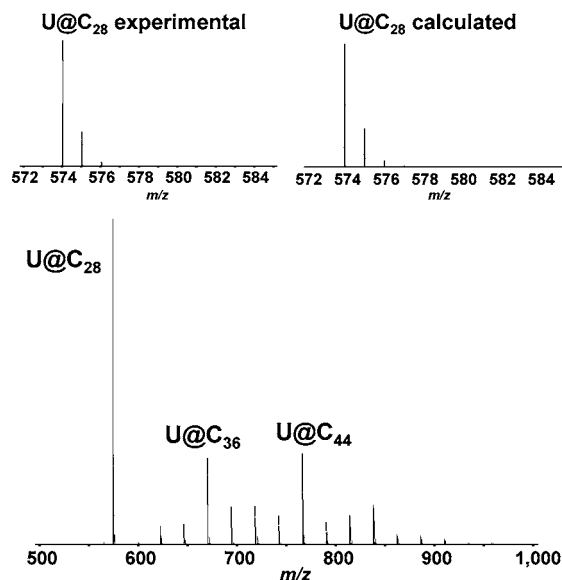

Figure 10. FT-ICR mass spectrum of cluster cations formed from vaporization of a UO$_2$-graphite target. U@C_{28} clearly forms directly from carbon vapor as a highly favored species.

vaporization of a UO$_2$-graphite (0.8 atom % U) target. U@C_{28} forms in high abundance, and its generation, and that of larger uranofullerenes, appears to be extremely efficient. CID experiments confirm that U@C_{28} is an endohedral metallofullerene (Figure S9, Supporting Information). Fragmentation of larger fullerenes, for example U@C_{32} or U@C_{38} (Figure S10 and S11, Supporting Information), shows C_2 loss with retention of the U atom to an end point of U@C_{28}.

The very strong formation of U@C_{28} from carbon vapor provides a rare opportunity to probe the fascinating processes of growth and initial formation of small endohedral fullerenes. Our recent experimental studies show that fullerenes primarily grow via a CNG mechanism in which atomic carbon and C_2 incorporate into closed-carbon networks of the fullerene cage.[33] In that work, higher fullerenes were examined exclusively, and they were shown to be the precursors of larger fullerenes. However, the smallest fullerene to form in carbon vapor, M@C_{28}, cannot form via the CNG mechanism. Thus, experimental

insight into how the smallest fullerene may form in carbon vapor remains a intriguing problem.[40]

To investigate the formation of U@C_{28} and the larger U@C_{2n} family, a UO_2-graphite target is vaporized in a series of experiments keeping all parameters constant except the helium pressure, as shown in Figure 11. It is known that only a narrow range of inert gas pressure allows efficient fullerene formation. Vaporization of the target at different helium pressures drastically affects formation and growth, and it should be possible to capture distinct stages of the growth process by varying the clustering conditions. That is achieved by firing the laser at different points along the helium pressure profile of the pulsed valve (800 μs width, backing pressure 70 psi).

At low helium pressures (conditions that yield low carbon vapor density and thus less clustering) in which the laser is fired well before the maximum of the pressure profile (Figure 11A), UO and UO_2 are primarily observed with little carbon cluster formation. Initially, U@C_{28} is weakly observed without the presence of larger U@C_{2n}. Notably, the fullerenes that form "magic number" clusters, such as U@C_{36} and U@C_{44} (as shown in Figure 10), are absent. The smallest fullerene, U@C_{28}, forms in greater abundance at higher pressure (Figure 11B,C); however, larger endohedral metallofullerenes are not present or begin to form very weakly. Figure 11D shows that U@C_{28} becomes much more dominant when vaporization of the target is performed at higher inert gas pressure. The larger endohedral uranofullerenes are still formed weakly, as evidenced by the low abundance of U@C_{36}. In Figure 11E, the laser is fired 1 ms after the pulsed valve opens. U@C_{28} becomes slightly more abundant, and the larger endohedral fullerenes are formed in considerably higher abundance. U@C_{36} is observed to become magic numbered. Vaporization at slightly longer time intervals after the gas pulse gives more optimal fullerene-generating conditions, and the cluster distribution shown in Figure 10 is reproduced, in which the larger uranofullerenes exhibit much greater abundances, with U@C_{36} and U@C_{44} favored. A key observation is that U@C_{28} is not formed by fragmentation of larger species during growth, but that it is first to form. The larger uranofullerenes form only after the smallest fullerene (U@C_{28}) is formed, in accordance with the CNG mechanism with U@C_{28} as the precursor or "gateway" species to the larger endohedral metallofullerenes. Carbon vapor density plays an important role in the efficient formation of the smallest fullerenes.

The dominant U@C_{28} fullerene forms before larger U@C_{2n} fullerenes and is likely the precursor or "gateway" species to those larger uranofullerenes. Now that we have demonstrated U@C_{28} forms directly from carbon vapor and not due to fragmentation of larger fullerenes, the problem of the initial formation mode of that smallest fullerene is investigated. There are two primary initial formation mechanisms for U@C_{28}: (1) top-down formation, in which a graphite fragment originating from the target is directly involved,[41] or (2) entirely bottom-up, in which the product is formed initially from small carbon clusters and atomic carbon. Previous investigations analyzing C_{60} formation have probed fullerene formation by the vaporization of targets comprised of ^{13}C-enriched amorphous carbon and graphite to gain insight into the growth process. They show that the amorphous carbon is incorporated into the fullerenes, and so small carbon clusters must have played a role in formation. However, incomplete incorporation of ^{13}C into the fullerenes is reported.[42] That observation allows a possible growth scenario in which the smallest fullerenes may directly
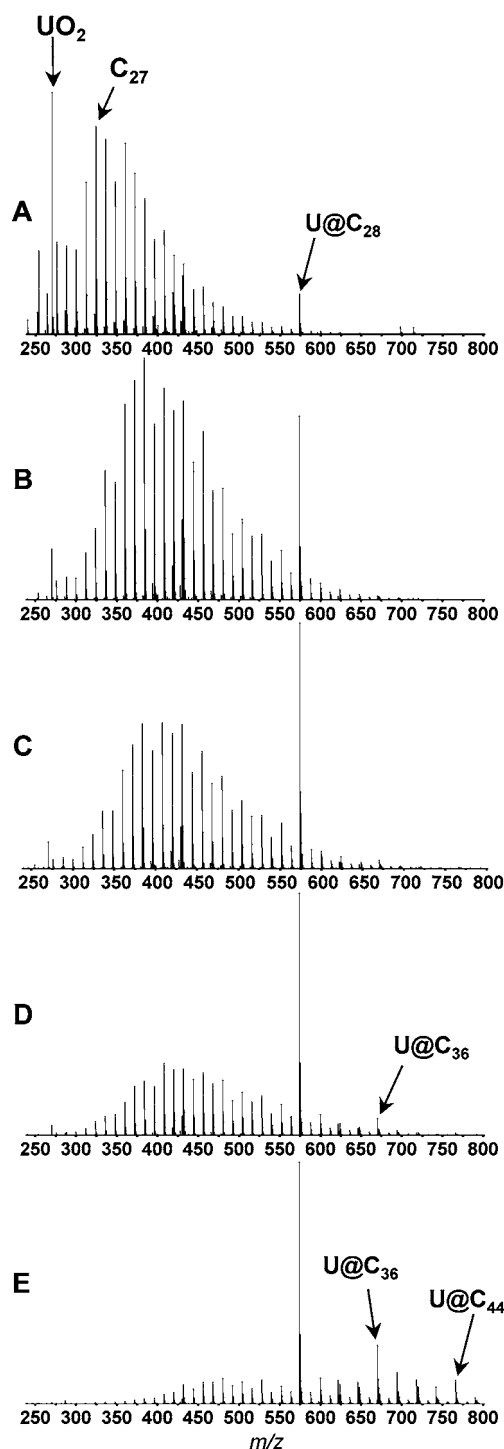

Figure 11. Results of laser vaporization of a UO_2-graphite target under increasing He gas pressure. U@C_{28} is demonstrated to form before larger U@C_{2n} endohedral metallofullerenes. Vaporization of the target rod at varying He pressures is achieved by firing the laser at different points in time along the pulse pressure profile. The laser is fired after the initial opening of the pulsed valve at several intervals of time to capture various stages of growth (70 psi He backing pressure, 800 μs pulse width): 400 (A), 600 (B), 700 (C), 800 (D), and 1000 μs (E).

form from graphitic fragments, and then further growth to larger fullerenes proceeds by the ingestion of small clusters and atomic carbon, as recently demonstrated experimentally for higher fullerenes.[33]

To distinguish between the two initial formation mechanisms, experiments are performed with a UO_2-graphite target enriched with ^{13}C amorphous carbon (99% ^{13}C) to provide a total of 10% ^{13}C of carbon in the target. Figure 12 shows the
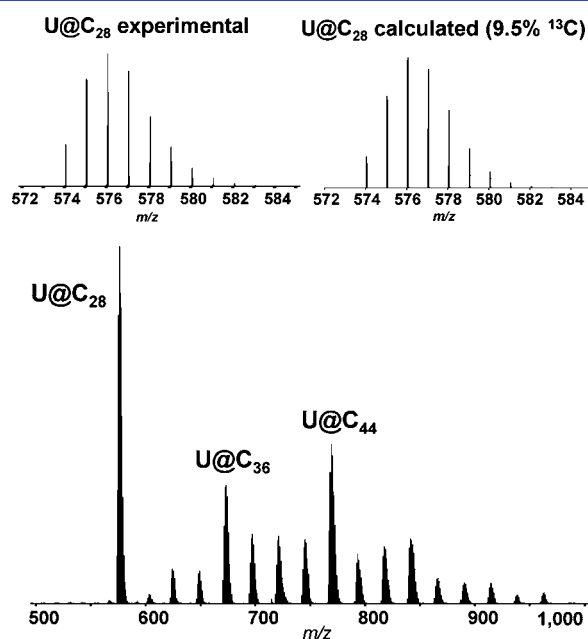

Figure 12. Results of laser vaporization of a composite rod comprised of UO_2 (0.8 atom %) and graphite, enriched with ^{13}C amorphous carbon to give a total ^{13}C content of 10 atom % of carbon. $U@C_{28}$ is shown to incorporate all enriched ^{13}C amorphous carbon, demonstrating that formation is bottom-up.

results of experiments in which clusters are formed by vaporization of that target under conditions identical to those in Figure 10. The resulting $U@C_{28}$ formed from the sample exhibits complete incorporation of the amorphous carbon. $U@C_{28}$ exhibits ^{13}C enrichment that varies between 9.5 and 10.5%, which appears to correspond to the statistical inhomogeneity of the amorphous carbon-graphite target. Thus, it is clearly demonstrated that $U@C_{28}$ forms bottom-up from atomic carbon and small carbon clusters under the present conditions. Further, uranium exhibits a particularly strong ability to catalyze or nucleate C_{28} formation.

CONCLUSIONS

Endohedral $M@C_{28}$ forms in carbon vapor as the smallest stable fullerene in the gas phase and represents a fundamental benchmark for further experimental and theoretical studies. $Ti@C_{28}$ appears to be the most stable of the $M@C_{28}$ family (M = group IV metals). The internally located Ti atom stabilizes the highly strained C_{28} cage by charge transfer. The ionic model has also been validated for other small fullerenes ($Ti@C_{30}$ and $Ti@C_{32}$). The transferred negative charge is preferentially localized in the [5,5] bonds and at the [5,5,5] carbon atom junctions, stabilizing the highly pyramidalized carbon atoms and enabling the $Ti@C_{28}$ species to resist further carbon insertion and thus growth to larger fullerenes via the CNG mechanism. Theoretical calculations further predict that the encapsulated Ti atom is also displaced toward the molecular zones where negative charge is localized, yielding further stabilization, indicating that covalent interactions also play an important factor. $Zr@C_{28}$ also forms in abundance, but $Hf@C_{28}$

is only weakly observed. The experimental detection of these species immediately opens the door to spectroscopic studies, and the nontoxic nature of Ti allows safe experimental attempts for its macroscopic synthesis. Additional exohedral stabilization of the most strained atoms may also be required to sufficiently stabilize the species in the solid state or in solution. Titanium encapsulation is demonstrated to be an attractive route toward synthesis of the smallest fullerenes that are not available as empty cages.

The results provide experimental insight into how endohedral fullerenes are formed in carbon vapor and allow for a complete description of fullerene formation to be developed. $U@C_{28}$ also exhibits strong formation in condensing carbon vapor and is demonstrated to form by a bottom-up growth mechanism. Larger $U@C_{2n}$ endohedral metallofullerenes are shown to form based on $U@C_{28}$ as their precursor. The growth mechanism is expected to apply to all other endohedral fullerenes and fullerenes as well. Thus, the smallest fullerene forms first, in which the encapsulating species are originally placed within the cage. Subsequent growth to larger endohedral fullerenes proceeds via the recently experimentally demonstrated CNG mechanism by incorporation of atomic carbon and C_2.[33] The encapsulating species nucleates or catalyzes initial endohedral fullerene formation, and it appears that particular elements or moieties are able to catalyze or nucleate formation to varying efficiencies. Uranium appears to be very efficient in catalyzing initial fullerene formation. The smallest endohedral fullerene to form will directly correlate to the properties of the encapsulating species. For example, the initial fullerene formed with a larger endohedral atom(s) or moiety may be larger than C_{28}. In addition, if an encapsulating species is small enough to form $M@C_{28}$, it must also stabilize C_{28} by charge transfer sufficiently to be observed, or all of the species may grow to larger fullerenes after initial formation in carbon vapor, or it may not be stable enough in the gas phase to detect. It may now be possible to decipher why certain elements more efficiently form endohedral fullerenes than those that are not able to form, or at least not readily form, endohedral fullerenes.

■ EXPERIMENTAL SECTION

Cluster Source. The cluster source blocks[33] are configured for use with 6.3 or 12.7 mm diameter target rods, which are simultaneously rotated and translated. A channel 2 mm in diameter and ∼8.5 mm in length runs from a pulsed valve (70 psi backing pressure, 800 μs pulse width) into the region containing the rod to introduce helium. A second channel 2 mm in diameter is directed into the target area to admit the laser beam. A channel 4 mm in diameter and ∼8.5 mm in length is located downstream from the target, aligned with the helium introduction channel to achieve confinement and clustering of the vapor produced. The gas then enters high vacuum and undergoes a free jet expansion. Vaporization of the target rod is achieved by a single laser shot fired from a Nd:YAG laser (532 nm, 3−5 ns, 5 mJ/pulse, ∼1.5 mm beam diameter) in conjunction with the opening of a pulsed valve to admit He into the source. Vaporization at various He pressures is achieved by adjusting the laser to fire at different intervals of time after opening the pulsed valve.

Graphite Targets. The 6.3 mm metal-doped graphite rods (0.8 atom % Ti, Hf, Zr) were manufactured by Toyo Tanso. The 12.7 mm rods are made by thoroughly mixing graphite powder (99.9995%, 2−15 μm) and the metal oxide (UO_2, TiO_2, ZrO_2, Hf_2O_3, >99.9% purity) to give metal-doped targets of 0.8 mol % metal oxide, and then molded into a composite rod by compressing the mixture in a press. See the Supporting Information for the full list of metals probed for $M@C_{28}$ formation. The ^{13}C-enriched uranium target is made by mixing 99%

^{13}C-enriched amorphous carbon, graphite powder, and UO_2 to give a rod that contains a total of 10 atom % ^{13}C and 0.4 atom % U.

9.4 T Fourier Transform Ion Cyclotron Mass Spectrometry. All experiments are analyzed with a custom-built FT-ICR mass spectrometer based on a 9.4 T, 155 mm bore diameter actively shielded superconducting magnet, and were conducted with positive ions. The cluster source is housed in a source chamber (1×10^{-7} Torr) evacuated by a large diffusion pump (3000 L/s). Ions produced in the cluster source are transported to the ICR cell via three stages of differential pumping, each supplied with a turbomolecular pump to achieve ultrahigh vacuum (10^{-10} Torr) in the ICR cell. After exiting the clustering region, the ions are skimmed into an octopole ion guide (175 V_{p-p}, 1.8 MHz, 570 mm length) and immediately transferred to a second octopole for ion accumulation. Ions are confined radially in the accumulation octopole (240 V_{p-p}, 2.8 MHz, 160 mm) by a time-varying electric field generated by a radiofrequency applied with 180° phase difference to adjacent rods and axially by the application of positive voltages to the end-caps at the conductance limits at either side of the accumulation octopole. Helium gas is introduced through a pulsed valve to the accumulation octopole ($\sim 10^{-4}$ Torr) to facilitate further ion cooling. After the accumulation of ions produced by 10 individual laser and helium pulse events, the ions are transferred by a third octopole (155 V_{p-p}, 2.2 MHz, 1450 mm) to an open cylindrical ion trap (70 mm diameter, 212 mm long, aspect ratio $\sim$2).[43] The ions are accelerated to a detectable cyclotron radius by a broadband frequency sweep excitation (260 V_{p-p}, 150 Hz/μs, 3.6 down to 0.071 MHz) and subsequently detected as the differential current induced between two opposed electrodes of the ICR cell. Each of the acquisitions is Hanning-apodized and zero-filled once prior to fast Fourier transform and magnitude calculation.[44] Ten time-domain acquisitions are averaged. The experimental event sequence is controlled by a modular ICR data acquisition system.[45]

SORI-CID. Ions are further probed by collision-induced dissociation. The ions of interest are isolated by applying a SWIFT event.[32] The selected ions are then subjected to a 10 ms pulse of helium or argon directly injected into the ICR cell via a pulsed valve located outside the magnet bore, followed by 250 μs single-frequency excitation at 1 kHz off-resonance.[32] After a 15–20 s delay to allow the system to re-establish base pressure, a broadband frequency sweep is carried out before detection. The mass spectrum is obtained from a single time-domain acquisition.

Computational Details. The calculations were carried out by DFT methodology with the ADF 2010 program.[46,47] The exchange-correlation functionals of Becke[48] and Perdew[49] were used. Relativistic corrections were included by means of the ZORA formalism. Slater triple-zeta + polarization basis sets were employed to describe the valence electrons of C and Sc. Frozen cores consisting of the 1s shell for C and the 1s to 2p shells for Ti were described by means of single Slater function.

■ ASSOCIATED CONTENT

Ⓢ Supporting Information

Complete list of metals probed for $M@C_{28}$ formation; ionization potentials and electron affinities for $Ti@C_{28}$, $Ti@C_{30}$, and $Ti@C_{32}$; fragmentation spectra for C_{27}, $Ti@C_{28}$, $Ti@C_{30}$, $Ti@C_{38}$, $U@C_{28}$, $U@C_{32}$, and $U@C_{38}$; spectrum of $Hf@C_{28}$ showing three different molecular ions near its nominal mass; and frontier orbitals for D_2-C_{28} and $Ti@D_2$-C_{28}. This material is available free of charge via the Internet at http://pubs.acs.org.

■ AUTHOR INFORMATION

Corresponding Author

kroto@chem.fsu.edu; marshall@magnet.fsu.edu; josepmaria.poblet@urv.cat

Notes

The authors declare no competing financial interest.

■ REFERENCES

(1) Kroto, H. W.; Heath, J. R.; Obrien, S. C.; Curl, R. F.; Smalley, R. E. *Nature* **1985**, *318*, 162−163.

(2) Van Orden, A.; Saykally, R. J. *Chem. Rev.* **1998**, *98*, 2313−2357.

(3) von Helden, G.; Hsu, M. T.; Kemper, P. R.; Bowers, M. T. *J. Chem. Phys.* **1991**, *95*, 3835−3837.

(4) von Helden, G.; Hsu, M. T.; Gotts, N.; Bowers, M. T. *J. Phys. Chem.* **1993**, *97*, 8182−8192.

(5) Kroto, H. W. *Nature* **1987**, *329*, 529−531.

(6) Breda, N.; Broglia, R. A.; Colo, G.; Onida, G.; Provasi, D.; Vigezzi, E. *Phys. Rev. B* **2000**, *62*, 130−133.

(7) Romero, N. A.; Kim, J.; Martin, R. M. *Phys. Rev. B* **2007**, *76*, e205405.

(8) Seifert, G.; Enyashin, A. N.; Heine, T. *Phys. Rev. B* **2005**, *72*, e012102.

(9) Enyashin, A.; Gemming, S.; Heine, T.; Seifert, G.; Zhechkov, L. *Phys. Chem. Chem. Phys.* **2006**, *8*, 3320−3325.

(10) Prinzbach, H.; Weller, A.; Landenberger, P.; Wahl, F.; Worth, J.; Scott, L. T.; Gelmont, M.; Olevano, D.; von Issendorff, B. *Nature* **2000**, *407*, 60−63.

(11) Kent, P. R. C.; Towler, M. D.; Needs, R. J.; Rajagopal, G. *Phys. Rev. B* **2000**, *62*, 15394−15397.

(12) Martin, J. M. L. *Chem. Phys. Lett.* **1996**, *255*, 1−6.

(13) Handschuh, H.; Gantefor, G.; Kessler, B.; Bechthold, P. S.; Eberhardt, W. *Phys. Rev. Lett.* **1995**, *74*, 1095−1098.

(14) Kietzmann, H.; Rochow, R.; Gantefor, G.; Eberhardt, W.; Vietze, K.; Seifert, G.; Fowler, P. W. *Phys. Rev. Lett.* **1998**, *81*, 5378−5381.

(15) Bowers, M. T.; Kemper, P. R.; von Helden, G.; Vankoppen, P. A. M. *Science* **1993**, *260*, 1446−1451.

(16) Cox, D. M.; Trevor, D. J.; Reichmann, K. C.; Kaldor, A. *J. Am. Chem. Soc.* **1986**, *108*, 2457−2458.

(17) Guo, T.; Diener, M. D.; Chai, Y.; Alford, M. J.; Haufler, R. E.; Mcclure, S. M.; Ohno, T.; Weaver, J. H.; Scuseria, G. E.; Smalley, R. E. *Science* **1992**, *257*, 1661−1664.

(18) Dognon, J. P.; Clavaguera, C.; Pyykko, P. *J. Am. Chem. Soc.* **2009**, *131*, 238−243.

(19) Sofronov, A. A.; Makurin, Y. N.; Gusev, A. I.; Ivanovsky, A. L. *Chem. Phys.* **2001**, *270*, 293−308.

(20) Zhao, K.; Pitzer, R. M. *J. Phys. Chem.* **1996**, *100*, 4798−4802.

(21) Guo, T.; Smalley, R. E.; Scuseria, G. E. *J. Chem. Phys.* **1993**, *99*, 352−359.

(22) Rosch, N.; Haberlen, O. D.; Dunlap, B. I. *Angew. Chem., Int. Ed. Engl.* **1993**, *32*, 108−110.

(23) Diener, M. D.; Smith, C. A.; Veirs, D. K. *Chem. Mater.* **1997**, *9*, 1773−1777.

(24) Akiyama, K.; Zhao, Y. L.; Sueki, K.; Tsukada, K.; Haba, H.; Nagame, Y.; Kodama, T.; Suzuki, S.; Ohtsuki, T.; Sakaguchi, M.; Kikuchi, K.; Katada, M.; Nakahara, H. *J. Am. Chem. Soc.* **2001**, *123*, 181−182.

(25) Tan, Y. Z.; Xie, S. Y.; Huang, R. B.; Zheng, L. S. *Nature Chem.* **2009**, *1*, 450−460.

(26) Wang, C. R.; Kai, T.; Tomiyama, T.; Yoshida, T.; Kobayashi, Y.; Nishibori, E.; Takata, M.; Sakata, M.; Shinohara, H. *Nature* **2000**, *408*, 426−427.

(27) Stevenson, S.; Fowler, P. W.; Heine, T.; Duchamp, J. C.; Rice, G.; Glass, T.; Harich, K.; Hajdu, E.; Bible, R.; Dorn, H. C. *Nature* **2000**, *408*, 427−428.

(28) Campanera, J. M.; Bo, C.; Poblet, J. M. *Angew. Chem., Int. Ed.* **2005**, *44*, 7230−7233.

(29) Rodriguez-Fortea, A.; Alegret, N.; Balch, A. L.; Poblet, J. M. *Nature Chem.* **2010**, *2*, 955−961.

(30) Klingeler, R.; Bechthold, P. S.; Neeb, M.; Eberhardt, W. *J. Chem. Phys.* **2000**, *113*, 1420−1425.

(31) Kimura, T.; Sugai, T.; Shinohara, H. *Int. J. Mass. Spectrom.* **1999**, *188*, 225−232.

(32) Marshall, A. G.; Hendrickson, C. L.; Jackson, G. S. *Mass Spectrom. Rev.* **1998**, *17*, 1−35.

(33) Dunk, P. W.; Kaiser, N. K.; Hendrickson, C. L.; Quinn, J. P.; Ewels, C. P.; Nakanishi, Y.; Sasaki, Y.; Shinohara, H.; Marshall, A. G.; Kroto, H. W. *Nat. Commun.* **2012**, *3*, 855 DOI: 10.1038/ncomms1853.

(34) Radi, P. P.; Bunn, T. L.; Kemper, P. R.; Molchan, M. E.; Bowers, M. T. *J. Chem. Phys.* **1988**, *88*, 2809−2814.

(35) Sowa, M. B.; Hintz, P. A.; Anderson, S. L. *J. Chem. Phys.* **1991**, *95*, 4719−4720.

(36) Fowler, P. W.; Manolopoulos, D. E. *An atlas of fullerenes*; Clarendon Press/Oxford University Press: Oxford/New York, 1995.

(37) Rodriguez-Fortea, A.; Balch, A. L.; Poblet, J. M. *Chem. Soc. Rev.* **2011**, *40*, 3551−3563.

(38) Slanina, Z.; Nagase, S. *Chemphyschem* **2005**, *6*, 2060−2063.

(39) Slanina, Z.; Lee, S. L.; Uhlik, F.; Adamowicz, L.; Nagase, S. *Theor. Chem. Acc.* **2007**, *117*, 315−322.

(40) Shelimov, K. B.; Jarrold, M. F. *J. Am. Chem. Soc.* **1996**, *118*, 1139−1147.

(41) Chuvilin, A.; Kaiser, U.; Bichoutskaia, E.; Besley, N. A.; Khlobystov, A. N. *Nature Chem.* **2010**, *2*, 450−453.

(42) Hawkins, J. M.; Meyer, A.; Loren, S.; Nunlist, R. *J. Am. Chem. Soc.* **1991**, *113*, 9394−9395.

(43) Beu, S. C.; Laude, D. A. *Int. J. Mass. Spectrom.* **1992**, *112*, 215−230.

(44) Marshall, A. G.; Verdun, F. R. *Fourier transforms in NMR, optical, and mass spectrometry: a user's handbook*; Elsevier: Amsterdam/New York, 1990.

(45) Blakney, G. T.; Hendrickson, C. L.; Marshall, A. G. *Int. J. Mass Spectrom.* **2011**, *306*, 246−252.

(46) Velde, G. T.; Bickelhaupt, F. M.; Baerends, E. J.; Guerra, C. F.; Van Gisbergen, S. J. A.; Snijders, J. G.; Ziegler, T. *J. Comput. Chem.* **2001**, *22*, 931−967.

(47) *ADF 2010*, 1st ed.; Department of Theoretical Chemistry, Vrije Universiteit: 2010.

(48) Becke, A. D. *Phys. Rev. A* **1988**, *38*, 3098−3100.

(49) Perdew, J. P. *Phys. Rev. B* **1986**, *33*, 8822−8824.

9389

dx.doi.org/10.1021/ja302398h | *J. Am. Chem. Soc.* 2012, 134, 9380−9389